Molecular Dynamics Investigation of the Structure of a Fully Hydrated Gel-Phase Dipalmitoylphosphatidylcholine Bilayer

Kechuan Tu, Douglas J. Tobias, J. Kent Blasie, and Michael L. Klein
Department of Chemistry, University of Pennsylvania, Philadelphia, Pennsylvania 19104-6323 USA

ABSTRACT We report the results of a constant pressure and temperature molecular dynamics simulation of a gel-phase dipalmitoylphosphatidylcholine bilayer with n_W = 11.8 water molecules/lipid at 19°C. The results of the simulation were compared in detail with a variety of x-ray and neutron diffraction data. The average positions of specific carbon atoms along the bilayer normal and the interlamellar spacing and electron density profile were in very good agreement with neutron and x-ray diffraction results. The area per lipid and the details of the in-plane hydrocarbon chain structure were in excellent agreement with wide-angle x-ray diffraction results. The only significant deviation is that the chains met in a pleated arrangement at the bilayer center, although they should be parallel. Novel discoveries made in the present work include the observation of a bimodal headgroup orientational distribution. Furthermore, we found that there are a significant number of *gauche* conformations near the ends of the hydrocarbon chains and, in addition to verifying a previous suggestion that there is partial rotational ordering in the hydrocarbon chains, that the two chains in a given molecule are inequivalent with respect to rotations. Finally, we have investigated the lipid/water interface and found that the water penetrates beneath the headgroups, but not as far as the carbonyl groups, that the phosphates are strongly hydrated almost exclusively at the nonesterified oxygen atoms, and that the hydration of the ammonium groups is more diffuse, with some water molecules concentrated in the grooves between the methyl groups.

INTRODUCTION

Fully hydrated bilayers of pure lipids have been used as model biological membranes in biophysical studies for many years. Several bilayer "phases" of hydrated phospholipids have been identified and structurally characterized (Small, 1986). These include the nearly dehydrated crystal (Pearson and Pascher, 1979), and crystalline L_c or "sub-gel" phases (Ruocco and Shipley, 1982); the $L_{\beta'}$ or "gel" phase in which the polar headgroups are disordered but the mostly all-*trans* hydrocarbon chains are tilted and pack in a regular two-dimensional array in the monolayer planes (Sun et al., 1994); the $P_{\beta'}$ rippled bilayer phase with hexagonally packed chains (Hentschel and Rustichelli, 1991); and the most biologically relevant L_α or "liquid crystal" phase, in which the chains are conformationally disordered and the lipid molecules are free to diffuse in the plane of the bilayer (Pfeiffer et al., 1989). The gel phase has been and continues to serve as a paradigm for experimentalists to study fully hydrated bilayers in a state containing sufficient order to allow quantitative structural work.

There have been many experimental studies of the structure of the gel phase in the last 20 or so years, with the main insight coming from neutron and x-ray diffraction experiments. Neutron diffraction experiments on selectively deuterated lipids has provided information on the average intramolecular configuration, namely the mean position of a particular deuterated chemical group (e.g., CD_2) along the bilayer normal (Büldt et al., 1979; Zaccai et al., 1979). X-ray diffraction has yielded complementary information on the average intermolecular configuration, e.g., the lateral organization of the lipids in the bilayers is probed by wide-angle diffraction (Levine, 1973). To extract a molecular picture from diffraction data, it is necessary to invoke a model. The models used to interpret x-ray data have attained increasing sophistication over the years. The most detailed to date is that of Sun et al. (1994), consisting of gaussian electron density distributions for the headgroups, and tilted rods of electron density for the hydrocarbon chains, which are assumed to be packed in a distorted hexagonal lattice and tilted toward nearest neighbors. The model contains a gap (methyl trough) in the middle of the bilayer and allows for separate offsets of the headgroups and chains in opposing monolayers.

In principle, molecular dynamics (MD) simulations can provide an atomic-scale picture of membrane structure that complements and assists in the interpretation of experimental results. Indeed, in the last few years, many reports of MD simulations of lipids have appeared in the literature. Two studies have focused on simulations of crystals of lecithin fragments for the purpose of evaluating force fields (Stouch et al., 1991; Tu et al., 1995a). The remainder have been concerned with the biologically more relevant liquid crystal bilayer phase (Damodaran et al., 1992; Venable et al., 1993; Heller et al., 1993; Stouch, 1993; Egberts et al., 1994; Huang et al., 1994; Robinson et al., 1994; Zhou and Schulten, 1995; Shinoda et al., 1995; Tu et al., 1995b). As we have stated previously (Tu et al., 1995a,b), in our view most of these simulations should be viewed cautiously because

Received for publication 28 June 1995 and in final form 10 November 1995.

Address reprint requests to Dr. Michael L. Klein, University of Pennsylvania, Laboratory for Research on the Structure of Matter, Philadelphia, PA 19104-6202. Tel.: 215-898-8571; Fax: 215-898-8296; E-mail: klein@lrsm.upenn.edu.

0006-3495/96/02/595/14 $2.00

the force fields were not adequately evaluated, and/or the simulations were too short to demonstrate convergence. Until now, the gel phase has been ignored by simulators, even though it presents a great opportunity to check the performance of a force field on a fully hydrated bilayer for which there exists a great deal of structural data, albeit not at the resolution of the crystals, but much more detailed than for the liquid crystal.

In this paper, we present results of a constant pressure and temperature (NPT) MD investigation of a dipalmitoylphosphatidylcholine (DPPC) bilayer with $n_W = 11.8$ water molecules/lipid molecule at 19°C. Under these and similar conditions of hydration and temperature, the lipids are known experimentally to be arranged in a fully hydrated, gel-phase bilayer structure (Small, 1986). We present a detailed comparison of our results to a wide variety of experimental structural data, thus validating the simulation, and point out some novel aspects of the gel-phase bilayer structure predicted by the simulation.

MATERIALS AND METHODS

The construction of the initial configuration for our contant NPT simulation involved a series of several set-up and equilibration stages. Starting with the coordinates of the two distinct molecules in the dimyristoylphosphatidylcholine (DMPC) x-ray crystal structure (Pearson and Pascher, 1979), we added two carbons to each hydrocarbon chain, used the space group operations and lattice translations of the crystal to generate a 4×8 monolayer of 32 DPPC molecules, adjusted the coordinates so that all of the phosphorus atoms were in the same (monolayer) plane to disrupt the crystal headgroup packing, and scaled the center-of-mass coordinates in the plane of the monolayer to give a surface area per lipid of 47.2 Å to satisfy experimental data on the gel phase (Tristram-Nagle et al., 1993). This monolayer was used as input to a 20-ps MD simulation (a time step of 1 fs was used in all of the calculations) with periodic boundary conditions at a constant temperature of 19°C. During this simulation the positions of the phosphorus atoms were held fixed and the hydrocarbon chain tilt angle evolved to 24°. A bilayer was constructed from the monolayer by using the symmetry operations of the DMPC crystal space group ($P2_1$), adjusting the interlayer separation so that the phosphorus-phosphorus distance was 45 Å, to be consistent with the experimental estimate for the gel phase from Wiener et al. (1989), and was subsequently subjected to 5-ps MD, again with fixed phosphorus atoms. A slab of bulk water with the same surface area as the monolayers was placed on each side of the bilayer. The thicknesses of the slabs were chosen to give $n_W = 11.8$. The length of the simulation cell in the direction of the bilayer normal (i.e., the interlamellar spacing) was gradually decreased in a series of 2-ps MD simulations (with fixed phosphorus atoms) to 63.4 Å, the value obtained by x-ray diffraction by Tristram-Nagle et al. (1993). The final stages of the equilibration included a 5-ps simulation of the resulting bilayer with fixed phosphorus atoms, followed by 25 ps with all of the atoms free.

After constructing and equilibrating the system as described above, we performed a 1070-ps MD simulation at constant external temperature (T_{ext} = 19°C) and pressure ($P_{ext} = 0$) in a fully flexible simulation box using the hybrid algorithm developed by Martyna et al. (1994). The extended system (ES) equations of motion were integrated by using an iterative Verlet-like algorithm. The SHAKE algorithm (Ryckaert et al., 1977) was used to constrain the lengths of bonds involving hydrogen atoms. The fictitious masses of the ES variables were chosen according to the prescription given by Martyna et al. (1994), with time scales of 0.5 ps for the thermostats and 1 ps for the volume and cell variables. The Nosé-Hoover thermostat chain length was five.

We employed the SPC/E water potential (Berendsen et al., 1987) and an all-atom lipid potential that we had tested previously in constant NPT MD simulations of crystals of the phospholipid fragments, dilauroylglycerol, and glycerylphosphorylcholine. The lipid potential was shown to reproduce well the experimental lattice constants and the molecular configurations and intermolecular interactions in the known x-ray crystal structures (Tu et al., 1995a). Periodic boundary conditions were applied in three dimensions to generate an infinite, multilamellar system, and the Ewald method was used to calculate the energies, forces, and virial due to the electrostatic interactions (Allen and Tildesley, 1989; Nosé and Klein, 1983). The minimum image convention was employed to calculate the van der Waals interactions and the real-space part of the Ewald sum with simple truncation at 10 Å (Allen and Tildesley, 1989). Long-range corrections to account for the truncated van der Waals interactions were included in the energies and pressures (Allen and Tildesley, 1989). The calculation was executed in parallel/vector mode on the Cray C90 computer at the Pittsburgh Supercomputing Center using the CHARMM program (Brooks et al., 1983), version 23, as modified by us to implement the ES dynamics, minimum image periodic boundary conditions, and Ewald summation.

Before turning to the results, we briefly comment on the choice of constant pressure ensemble used in this work. The constant NPT MD algorithm used here is one where the lengths of the axes defining the simulation box, as well as the angles between the axes, are allowed to fluctuate such that, on average, the components of the pressure tensor satisfy $P_{\alpha\beta} = P_{ext}\,\delta_{\alpha\beta}$, where P_{ext} is the extonal pressure, i.e., there is no surface tension in the system. The set-up and boundary conditions of the simulation were chosen to represent, on the molecular scale, a portion of the multilamellar vesicles or planar-oriented bilayer samples used in the experiments to which we compare our results. It has been suggested recently, by analogy with alkane/water interfaces and insoluble monolayers at the air/water interface, that there is a nonzero surface tension at the lipid/water interface in bilayer phases, and that this tension must be accounted for in constant-pressure simulations of lipid bilayers (Chiu et al., 1995; Feller et al., 1995). Under the conditions of temperature and hydration chosen for our simulation, the DPPC/water phase diagram indicates that the simulated system should be in a single, continuous thermodynamic phase, namely a fully hydrated $L_{\beta'}$ lamellar bilayer phase (Small, 1986). In such a single-phase system, there cannot be surface tension in a true thermodynamic sense, for otherwise the system would separate into more than one phase at equilibrium.

There appears to be some confusion about the relevance of "surface tension" as applied to a single thermodynamic phase such as a multilamellar system. To alleviate the confusion, it is useful to consider the relevant energy scales in the problem (Safran, 1994). Thermodynamically, the surface tension is defined as the derivative of the free energy with respect to the area (per molecule). In a bulk, membrane-type system at equilibrium, the molecules adjust their area such that the free energy is a minimum, i.e., the surface tension vanishes. There can be deformations in the area per molecule from this minimum, but these are typically of higher energy than curvature deformations, those perturbations that do not change the overall volume of the membrane. This is different from the case of a system such as an insoluble (Langmuir) monolayer at the air/water interface where, because of the confining geometry, the area/molecule is generally different from that which gives a vanishing surface tension.

RESULTS AND DISCUSSION

The time evolution of the interlamellar spacing and surface area per lipid during the constant NPT simulation are shown in Fig. 1 *a*, and the hydrocarbon chain tilt angle and tilt direction are shown in Fig. 1 *b*. Here, the tilt angle is defined as the angle between the bilayer normal and a vector drawn from the fourth to the twelfth carbons in an acyl chain, and the tilt direction is the angle between the projection of that vector and the x axis of the simulation cell in the plane of the bilayer. The results in Fig. 1 indicate that it took 350 ps for the tilt angle to equilibrate, and 550 ps for the lamellar

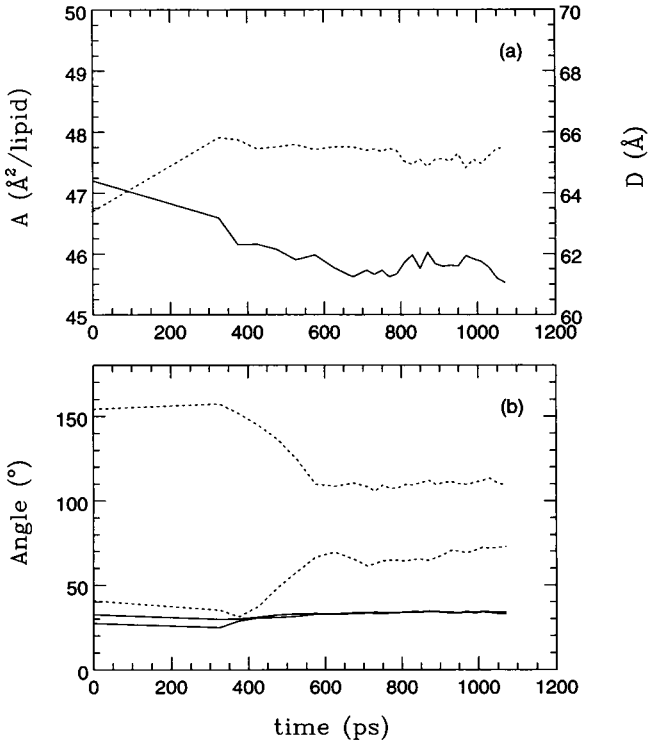

FIGURE 1 Time evolution of important structural measures during the constant NPT MD simulation of gel phase DPPC. (*a*) Area/lipid *A* (*solid line*) and interlamellar spacing *D* (*dashed line*). (*b*) Hydrocarbon chain tilt angle with respect to the bilayer normal (*solid lines*) and tilt direction with respect to the *x* axis (*dashed lines*) in the two halves of the bilayer.

spacing, area per lipid, and tilt direction to stabilize. Thus, our analysis is based on the last 500 ps of the simulation. The lamellar spacing, D, and area per lipid, A, did not change appreciably from their initial values, but the chains established a $\theta_t \approx 30°$ tilt in roughly the nearest-neighbor direction (see below) during the equilibration period. The average values calculated over the last 500 ps of the simulation are compared in Table 1 to results from the x-ray diffraction experiments of Tristram-Nagle et al. (1993). The area per molecule from the simulation is about 3% too low, and interlamellar spacing about 3% too high, but the density of the system is correct. The average value of the tilt angle from the simulation is very close to that extracted from the diffraction data.

In Table 2 we show the average values of the scalar internal pressure, P_{int}, as well as its components, P_N and P_T, normal and tangential, respectively, to the bilayer, and the

TABLE 1 Comparison of MD and experimental results for the area per lipid (A), lamellar spacing (*D*), and tilt angle (θ_t) in gel phase DPPC at 19°C and n_w = 11.8 waters/lipid

Quantity	MD	Expt.*
A (Å²/lipid)	45.8	47.2 ± 0.5
D (Å)	65.2	63.4 ± 0.3
θ_t (°)	33.6	32.0 ± 0.5

*Tristram-Nagle et al., 1993.

TABLE 2 Average pressures and surface tension from the simulation

$\langle P_{int} \rangle$ (atm.)	−6.7 ± 11.1
$\langle P_N \rangle$ (atm.)	−5.1 ± 17.0
$\langle P_T \rangle$ (atm.)	−7.5 ± 11.7
γ (dyne/cm)	0.6 ± 6.4

Uncertainties are $2\sigma/n_b^{1/2}$, where σ is the standard deviation of n_b block averages (using a block size of 1 ps).

surface tension, $\gamma = \langle D(P_N - P_T)/2 \rangle$ (Feller et al., 1995). As expected from the discussion at the end of Materials and Methods, the internal pressure and surface tension are close to zero (well within the statistical uncertainty).

An instantaneous configuration from the simulation is shown in Fig. 2. This figure illustrates many aspects of the gel-phase bilayer structure, which was stable throughout the simulation, and we will refer to it occasionally as we develop a structural picture through the analysis that follows.

Neutron diffraction experiments on selectively deuterated lipids have been used to map the profile structures along the bilayer normal of gel-phase bilayers (Büldt et al., 1979; Zaccai et al., 1979). The experimental data reduction involves fitting the observed structure factors, assuming gaussian distributions for the labeled segments from which the average positions along the normal can be extracted with an accuracy of ±1 Å. We have computed average distances of various atoms from the bilayer center along the bilayer normal and compare them in Table 3 to results from neutron

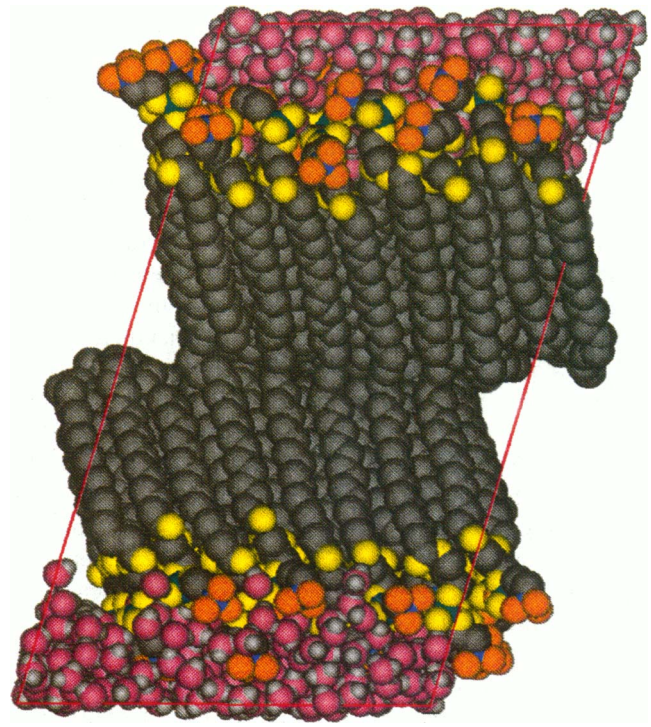

FIGURE 2 Instantaneous configuration from the MD simulation. Coloring scheme: C, gray, except ammonium C orange; N, blue; P, green; lipid O, yellow; water O, pink; water H, white (H atoms on the lipid molecules are omitted for clarity). The simulation cell is outlined in red.

TABLE 3 Comparison of MD and experimental results for the distances from the bilayer center along the bilayer normal*

Atom‡	MD	Expt.§
C_α	24.5	24.4 ± 0.6
C_β	23.7	24.1 ± 1.0
C_γ	23.4	23.6 ± 1.0
GC–3	20.7	21.6 ± 1.5
C4	14.3	15.4 ± 1.5
C5	13.3	13.7 ± 1.5
C9	9.1	9.8 ± 1.0
C14	3.8	4.1 ± 1.0
C15	2.8	2.5 ± 1.0

*Distances in Å.
‡The nomenclature is that of Büldt et al. (1979), i.e., —$C_{GC\text{-}3}H_2$—O—P—O—$C_\alpha H_2$—$C_\beta H_2$—$N(C_\gamma H_3)_3$, and C_n is the nth carbon in a hydrocarbon chain where the numbering begins at the carbonyl carbon.
§Büldt et al., 1979.

diffraction experiments on a similar system to evaluate the quality of the time-averaged structure from our simulation. The agreement between the simulation and experimental results is excellent, with the simulation values falling within the experimental uncertainties for all of the labeled positions. The observation that the three labeled carbon atoms in the choline group have almost the same value implies that the headgroups are aligned approximately parallel to the bilayer plane. From the MD trajectory we found that the average angle between the P-N vector and the bilayer plane is 20°, pointing into the water layer.

The atomic-scale resolution of the simulation can be used to assess the validity of the assumptions used in the experimental data reduction, namely, the use of gaussian distributions for the label positions. For many atoms we found a distribution like that of GC-3 in Fig. 3 *a*, i.e., a sharply peaked, unimodal distribution with a shoulder. Such a distribution could be fit reasonably well with a gaussian distribution. However, for the carbons in the ammonium methyl groups we obtained broad, bimodal distributions, indicating two dominant configurations of the phosphocholine headgroup. Indeed, closer inspection of the distribution of the P-N dipole inclination angle reveals that there are two roughly equal populations with angles 6° and 49°, respectively, that give rise to the average value of 20° (these may be discerned in Fig. 2). The simulation suggests that the use of a single gaussian for the chain carbon distributions also appears to be unjustified. The distributions for the chain carbons shown in Fig. 3 *b* show that the same carbons in different chains of a given molecule are inequivalent, i.e., they are out of step, by 1.0–1.8 Å. This inequivalence was observed previously in the neutron data of Zaccai et al. (1979), where it was found that the second carbon of the *sn*-2 chain was offset by 1.8 Å (away from the bilayer center) relative to that of the *sn*-1 chain. The simulation data add to the picture by showing that the inequivalence not only manifests itself in the mean positions of the carbons, but also in the widths of the distributions: the distributions of the carbons in the *sn*-1 chains are consistently almost

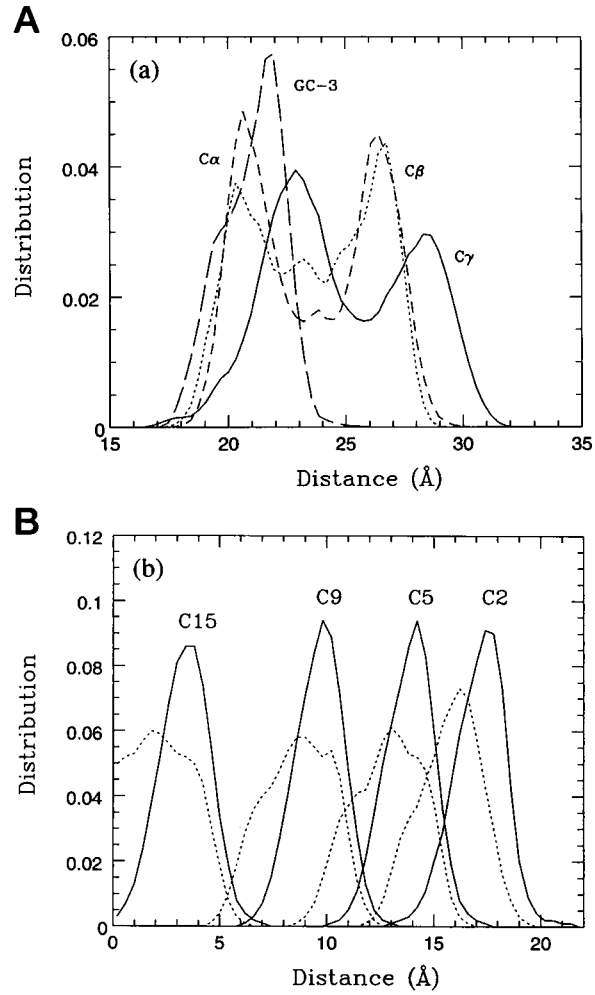

FIGURE 3 The number density profiles as functions of distance from the center of the bilayer along the bilayer normal (*a*) headgroup segments. (b) Selected segments in the *sn*-1 (*dashed lines*) and *sn*-2 (*solid lines*) hydrocarbon chains. See Table 3 for nomenclature.

twice as broad as those in the *sn*-2 chains. Thus, we conclude that the *sn*-2 chains are more rigidly held in place than the *sn*-1 chains. We will have more to say about the chain inequivalence below.

Low-angle x-ray diffraction is a complimentary method to neutron diffraction for measuring the profile structure of lipid bilayers. The structure is determined by fitting a model electron density profile to the observed structure factors. The most extensive analysis of low-angle diffraction data to date on gel-phase bilayers is that of Wiener et al. (1989). These authors combined various experimental data (volumetric, and low- and wide-angle diffraction) in a self-consistent electron density modeling procedure. The most appealing model from that study, the "2G hybrid" model, is one in which the headgroup region is represented by two gaussians, the terminal methyl region in the center of the bilayer by an inverted gaussian, with flat methylene and water regions, all continuously connected by bridging functions. We have computed the electron density profile from

the simulation data by placing a gaussian distribution of electrons on each atomic center with a variance equal to the van der Waals radius, for each configuration, and averaging over configurations. The resulting electron density profile in Fig. 4 bears a striking resemblance to the 2G model of Wiener et al.: there is a broad, asymmetric double peak in the headgroup/glycerol region, a flat methylene region, and a distinct terminal methyl trough. The distance between the maxima, 45.6 ± 0.8 Å, agrees very well with the experimental value, 45.0 ± 1.0 Å (Wiener et al., 1989).

Wiener et al. pointed out that the electron density models that gave the best fits to the experimental data were those in which two features were included in the headgroup/glycerol region. The split peak in the region of the polar group has been known for some time (Lesslauer et al., 1972). The interpretation given, based on lamellar x-ray and neutron diffraction (the latter employing H_2O-D_2O exchange to locate bound water molecules), was that the maximum in the electron density profile was due to the solvated phosphocholine group, and the inner shoulder to the acyl ester groups plus ≈ 0.7 water molecules per lipid (Lesslauer et al., 1972; Zaccai et al., 1975). We have used the simulation data to dissect the electron density profile into atomic contributions. The right side of Fig. 4 shows the contributions from the polar region, i.e., the phosphate, ammonium, and the two glycerol ester groups. The position of the phosphate group (PO_4) coincides with the maximum in the overall profile, and the ester groups with the shoulder of the peak. The electron density of the ammonium group displays two peaks, as expected from the nuclear density profile in Fig. 3 *a*. The left side of Fig. 4 separates the DPPC and water contributions. The peak in the DPPC profile actually coincides with the glycerol ester groups rather than at the high-electron-density phosphate region. The water electron density has its maximum between the bilayers, and it rapidly decreases in the ammonium region, flattens at the phosphate group, and then rapidly decays to zero in the glycerol region. Comparing the left and right sides of the figure, we see that it is the combination of the electron density of the phosphate group and its water of hydration that gives rise to the maximum in the overall profile. The glycerol region is only weakly hydrated compared to the phosphate groups, and the acyl ester groups are dry (see Fig. 2). The latter observation signals a slight discrepancy between the MD and experimental data: the neutron work, in particular, clearly shows that there is a bound water site corresponding to about 0.7 molecules around 16 Å, and this is on the inside (toward the bilayer center) of the shoulder of the peaks in both the x-ray and MD electron density profiles, whereas the water density is zero inside 20 Å on the MD profile. Solvation analysis (see below) reveals that there is 0.5 water molecule within 4.5 Å of each ester carbonyl group, and the electron density profile dictates that it must be located away from the bilayer center with respect to the ester group. In spite of the fact that the simulation misplaces the water, it does add to the interpretation of the shoulder at 18 Å, namely, the shoulder arises primarily from the ester groups whose electron densities are peaked at 17–18 Å, rather than the ester groups plus bound water as previously suggested. Evidently, the 0.7 water at 16 Å does not contribute appreciably to the x-ray scattering. Incidentally, the observation that the water inside the ester groups is misplaced in the simulation could explain why the MD area per lipid is slightly low (by about 1.5 $Å^2$).

We have used the MD trajectory to calculate the structure factor for the hydrocarbon chains only (because the headgroups are disordered (Sun et al., 1994; also see below)). We have plotted the spherically averaged structure factor in Fig. 5 as a function of the scattering angle, 2θ, and the cylindrically averaged structure factor in Fig. 6 as a function

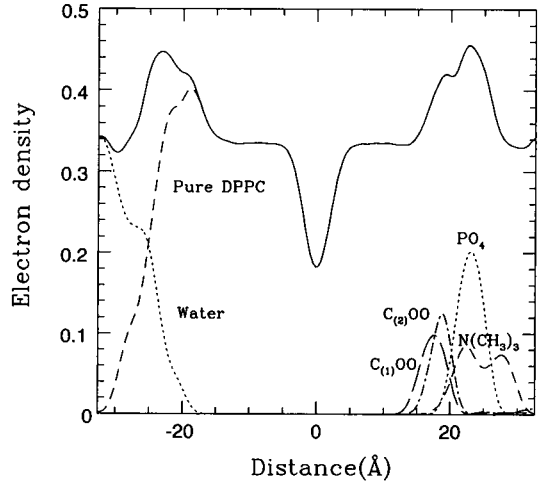

FIGURE 4 Electron density profiles along the bilayer normal, z, averaged over the simulation. The solid line is the total electron density. The broken lines on the left side of the figure show the separate contributions from the DPPC and water molecules, respectively, and on the right side contributions from chemical moieties in the headgroup and acyl ester regions of the DPPC molecules.

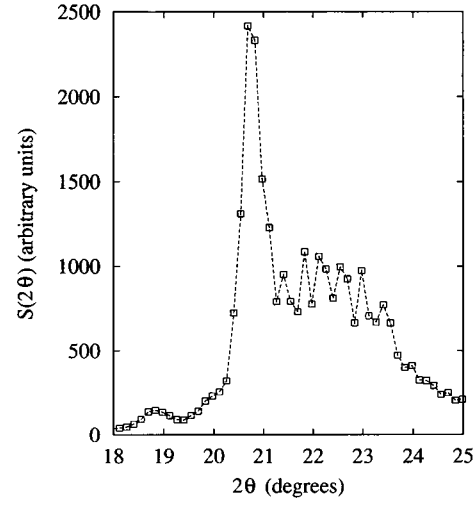

FIGURE 5 Spherically averaged hydrocarbon chain structure factor, $S(2\theta)$. There is a sharp (20) peak centered at $2\theta = 20.7$ and a broad (11) peak between roughly 21 and 23.5°.

of the in-plane and normal components, q_r and q_z, respectively, of the momentum transfer vector. There are several points of agreement and some of disagreement between the calculated and experimentally measured structure factors. We begin with the agreement.

As in the experimental wide-angle x-ray diffraction data on unoriented (powder) samples (Sun et al., 1994), there is a sharp (20) peak (whose width is limited by the system size) and a broad (11) peak (see Fig. 5) in the spherically averaged $S(2\theta)$. The cylindrically averaged $S(q_r,q_z)$ contains a set of (20) peaks and two sets of (11) peaks. The positions of the (20) and major (11) peaks in Fig. 6 correspond to d_{20} = 4.3 and d_{11} = 4.1 Å. Thus, we found that the chains pack primarily in a distorted hexagonal (orthorhombic) two-dimensional lattice with the unit cell parameters a_c = 8.6 and b_c = 4.7 Å (see Fig. 7). For comparison, x-ray diffraction data give d_{20} = 4.24 and d_{11} = 4.18 Å, corresponding to a_c = 8.5 and b_c = 4.8 Å, at 24°C (Sun et al., 1994), and d_{11} = 4.14 Å at 19°C (Tristram-Nagle et al., 1993). The major (20) peaks in Fig. 6 occur roughly at $q_z = \pm 0.1$ Å^{-1}, and this implies that the chains tilt between the neighbors, but more toward nearest neighbors (NN) (Kenn et al., 1991; Smith et al., 1988) (see Fig. 7). The tilt angle, θ_t, defined with respect to the bilayer normal, and tilt direction, ϕ_t, defined here with respect to the (11) direction in reciprocal space, can also be calculated from the relative position of the (20) and (11) peaks by assuming that the chains are cylinders (Kenn et al., 1991). The major peaks in Fig. 6 yield θ_t = 33.4° and ϕ_t = 23.2°. Direct calculation from the MD trajectory, with θ_t defined as the angle between the bilayer normal and the C4-C12 vector, gives 33.6°. The experimentally derived tilt angle is around 32°, toward nearest neighbors, i.e., $\phi_t \approx 30°$ (Tristram-Nagle et al., 1993; Sun et al., 1994). The small disagreement in the tilt direction is no surprise. Indeed, x-ray studies on free-standing DMPC films show that the tilt direction can be NN, toward the next nearest neighbors (NNN), i.e., $\phi_t \approx 0°$, or between the nearest neighbors, depending on the hydration level (Smith et al., 1988). In another x-ray diffraction experiment on oriented DPPC multilayers, NNN tilt was observed at 0% humidity, and ϕ_t = 24° was found at higher

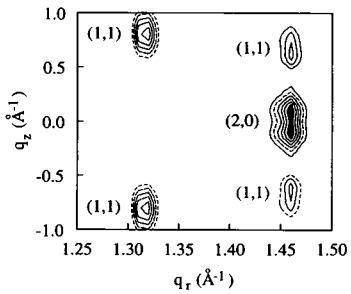

FIGURE 6 Cylindrically averaged hydrocarbon chain structure factor, $S(q_r,q_z)$. There is one set of (20) peaks and two sets of (11) peaks. The (20) peaks are at (1.46, ± 0.1), the major (11) peaks at (q_r,q_z) = (1.32, ± 0.8), and the minor (11) peaks at (1.46, ± 0.6) Å^{-1}. The apparent spreading of the peaks in the q_r direction is due to the difference in the q_r and q_z scales.

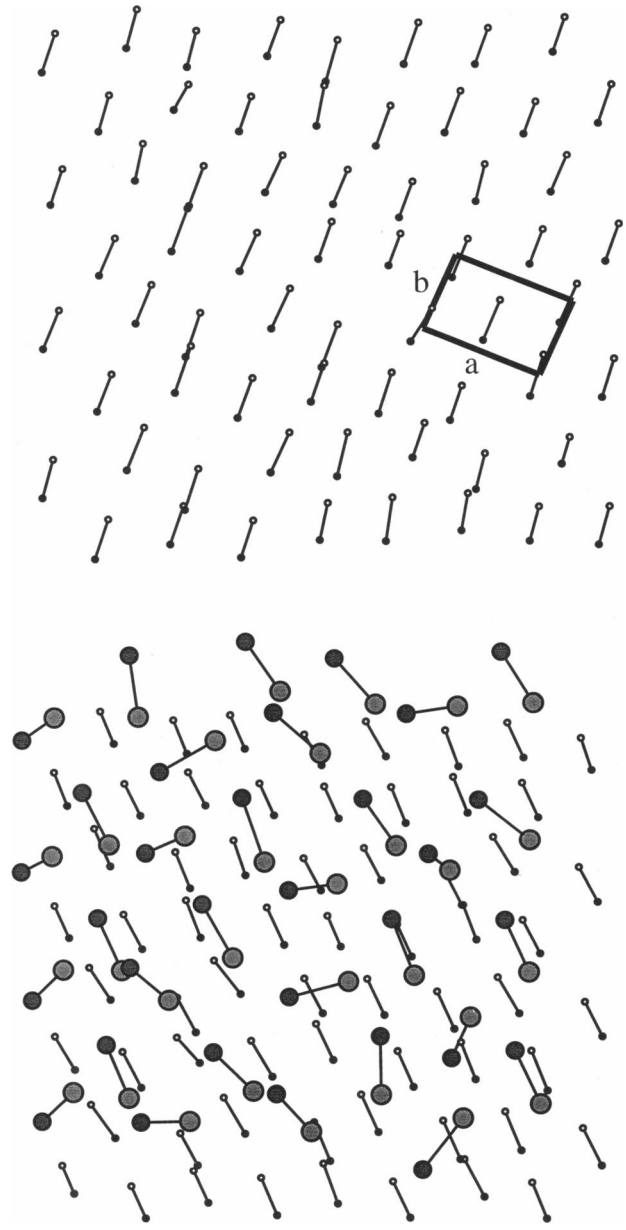

FIGURE 7 Projections of hydrocarbon chain C4 (*filled*)-C8 (*open*) vectors of each monolayer onto the bilayer plane from a 20 ps average structure. On average, the chains pack primarily in a distorted hexagonal (orthorhombic) lattice whose unit cell, is indicated in the upper half of the figure (note $a = a_c$, $b = b_c/\cos\theta_t$). Note the mirror-image relationship between projections of the chains in the two monolayers. The projections of headgroup P-N vectors are superposed on the lower half of the figure. The P atoms are denoted by the dark large circles and N atoms by the light large circles. Note the disorder in the headgroup structure.

hydration (Katsaras et al., 1992). To summarize the discussion of the hydrocarbon chain structure thus far, the main features of the calculated structure factors, and the implied structure, are in very good agreement with x-ray diffraction results. Now we turn to the points of disagreement and their structural implications.

The main point of disagreement between the spherically averaged structure factor in Fig. 5 and the experimental

powder diffraction data (Sun et al., 1994) is that the (11) peak in the simulation data is too wide by a factor of about 2. Looking at the cylindrically averaged pattern in Fig. 6, it is evident that there are two contributions to the additional broadness of the (11) peak in the spherically averaged pattern. One is the extra set of minor (11) peaks that occur at $(q_r,q_z) = (1.46, \pm 0.6)$ Å^{-1}, and contribute to intensity centered around 22.3° in $S(2\theta)$. These peaks are present regardless of whether a bilayer or isolated monolayers are used in the calculation of the structure factors from the simulation and in model calculations (Tu et al., manuscript in preparation), and we attribute them to a "monoclinic distortion" of the orthorhombic chain lattice (i.e., $\delta \neq 90°$, where δ is the angle between the a and b axes). The distortion causes $d_{11} = d_{-1-1} \neq d_{-11} = d_{1-1}$ and, hence, a splitting of the (11) peaks. In general, the splitting will involve a change in both q_r and q_z, but, in the present case, the distortion does not disrupt the orthorhombic symmetry (on the average) of the simulation box, and this symmetry causes the (20) and minor (11) peaks to occur at the same q_r.

The second contribution to the enhanced width of the (11) peak in $S(2\theta)$ is the spread of the major (11) peaks in the q_z direction in $S(q_r,q_z)$. We have identified two possible origins of this q_z spread and have used the model calculations to explore their consequences. One possible origin is a "static" tilt disorder, i.e., a distribution of tilt angles at each instant of time. Considering the intersection of the hydrocarbon chain form factor (essentially a disk modulated by a sinc function, i.e., the Fourier transform of the roughly cylindrical chain electron density (Hui, 1976; Sun et al., 1994)) with the Bragg rods, the effect of tilt disorder (distribution of tilt angles in the NN direction) is to spread the intensity along the (11) rods, with no effect on the (20) rods (if the tilt distribution is restricted to the NN direction). By examining the tilt distributions in individual configurations, we have identified static tilt disorder in the simulation (this is somewhat evident in Figs. 7 and 8). The probability distribution of the tilt angle calculated from the simulation has a Gaussian shape with a half-width at half-maximum of about 5°. This value is significantly higher than the 1.3° estimated from x-ray diffraction data (Sun et al., 1994). We have incorporated the tilt angle distribution from the simulation into the model calculations of the structure factors and found that the tilt disorder accounts for only a small fraction of the q_z spread of the (11) peak in $S(q_r,q_z)$ and enhanced width of the (11) peak in $S(2\theta)$ observed in the MD results.

Another possible origin of the q_z spread is that the chains in the two monolayers are not parallel. One can see in the configurations shown in Fig. 8 that the two layers actually pleat toward each other. The projections onto the bilayer plane show that the hydrocarbon chains from the two monolayers have a mirror image relationship (see Fig. 7). This pleated structure persisted throughout the simulation, even though the tilt angle and direction changed. The intrinsic (no tilt disorder) q_z spread is determined by the "thickness" of the form factor, which is inversely proportional to the length of the scattering unit in the z direction. Thus, we expect the intrinsic q_z spread due to scattering from the pleated structure, in which the independent scattering unit is a monolayer, to be twice that of the parallel chain structure, in which the scattering unit is the bilayer. The model calculations show that most of the q_z spread arises from the pleated chain structure. Moreover, the pleating indirectly accounts for the extra, minor (11) peaks, because there is no way to accommodate two pleated monolayers in the same simulation cell without distorting the orthorhombic lattice.

In summary, the main disagreement between the calculated and observed wide-angle scattering, i.e., the width of the (11) peak in $S(2\theta)$, primarily arises because of the occurrence of a pleated bilayer structure in the MD simulation. In spite of this problem, the simulation quantitatively

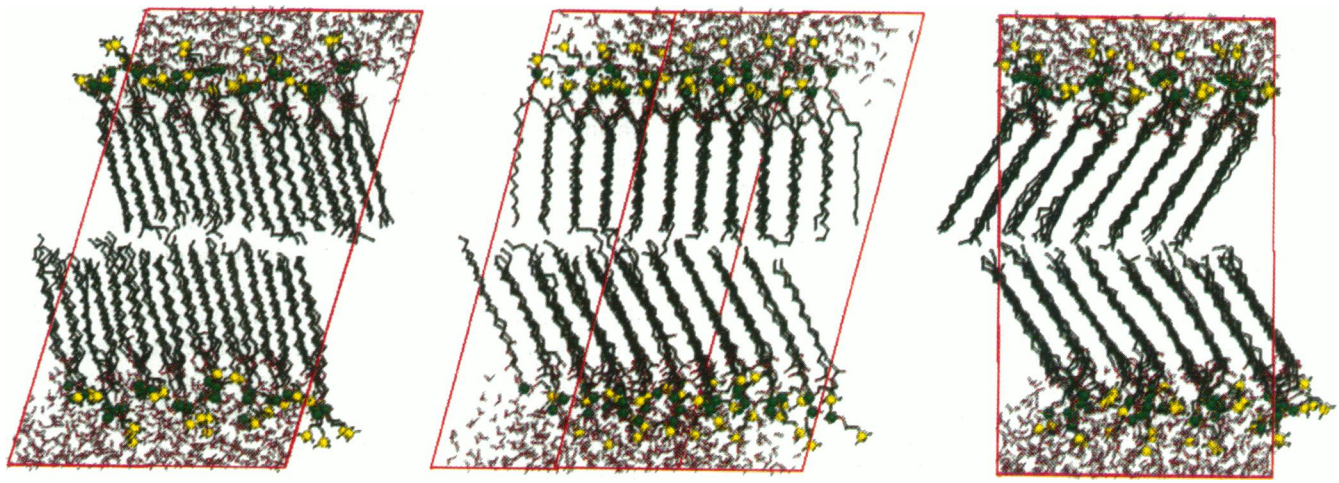

FIGURE 8 Three views (differing by rotation about the bilayer normal) of an instantaneous configuration from the MD simulation. Coloring scheme: C, black; N, yellow; P, green; O, red; water H, gray (H atoms on the lipid molecules are omitted for clarity). The simulation cell is outlined in red. Note the offsets and pleated arrangement of the chains in opposing layers.

reproduces the in-plane structure of the hydrocarbon chains within a monolayer. There are two possible explanations for the persistence of the pleated structure in the simulation. One is that there is a subtle deficiency in the hydrocarbon chain potential that gives the pleated structure as the free energy minimum. Another is that the pleated structure is a local minimum in which the simulation becomes trapped. Indeed, the simulation was initiated using a pleated bilayer configuration. We are currently performing additional calculations to discern between the possible explanations.

Until recently, the gel phase was considered as a tilted bilayer structure with colinearity of pairs of chains from the opposing monolayers (Hui, 1976), i.e., the chains meet end to end in the middle of the bilayer. To fit the wide-angle x-ray data, Sun et al. (1994) relaxed this constraint and allowed for the two monolayers to have an offset in the bilayer plane. We found that the chain offset indeed exists in our simulation, as can be seen in Fig. 8. The projections of the chain ends onto the bilayer plane from a 20-ps averaged configuration are shown in Fig. 9. The figure shows that the chains are not offset in a regular fashion in the simulation, in contrast to the model of Sun et al. The average in-plane distance between chains in opposing layers calculated from the MD trajectory is 0.82 Å, compared to 0.79 Å in the model of Sun et al.

Next we examine the conformational preferences that permit the tilted hydrocarbon chain structure. Fig. 10 shows the dihedral angle distributions in the two acyl ester linkages. The $\gamma 2/\beta 2$ and $\gamma 4/\beta 4$ pairs of dihedral angles (see Fig. 11 for notation) in both chains display sharp, unimodal distributions corresponding to *trans/trans* conformations. The $\gamma 1/\beta 1$ and $\gamma 3/\beta 3$ pairs of dihedral angles each have two

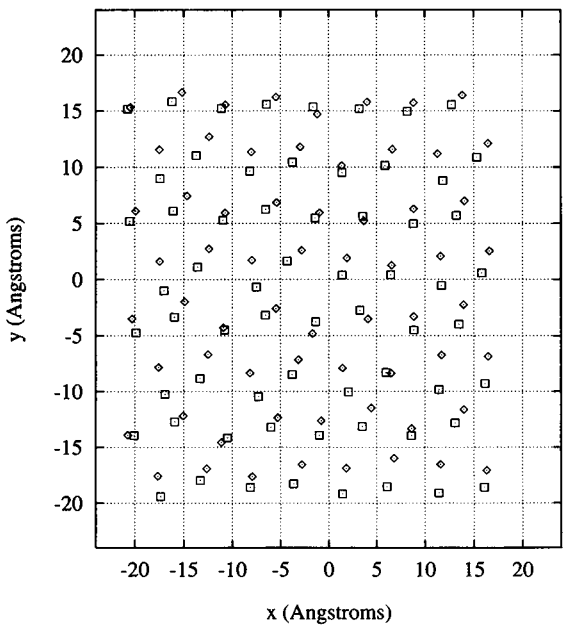

FIGURE 9 Projections of the chain ends onto the bilayer plane in an average configuration taken over 20 ps. The chains in opposing layers are represented by squares and diamonds, respectively.

predominantly distinct populations that are strongly correlated. In the *sn*-1 chain, the major *trans* $\gamma 1$ population is correlated with the *gauche*$^-$ conformation at $\gamma 3$, and the minor $\gamma 1$ population around 80° with the *gauche*$^+$ conformation at $\gamma 3$. Both of these sets of conformational preferences give a tilted *sn*-1 chain. The case corresponding to the major population was predicted by Hauser et al. (1981), whereas the minor population appears to be a novel observation from the simulation. The acyl linkage of the *sn*-2 chain also has two conformations that permit it to be tilted parallel to the *sn*-1 chain. The major population has the $\beta 1$ and $\beta 3$ dihedrals bent at roughly right angles (90° and 270°, respectively), and a minor population has $\beta 1 \approx 120°$ and $\beta 3$ bent slightly from *trans*. Fig. 12 shows how an essentially untilted structure in the DMPC crystal (Fig. 12 *a*) can be converted to the two tilted gel-phase structures by modifying the dihedral angles in the acyl ester regions to the two sets of preferred values from the simulation (Fig. 12, *c* and *d*, respectively). The only significant differences in dihedral angles between the two conformations in the gel phase and the two molecules in the DMPC crystal are in $\gamma 3$ (*gauche* in the gel versus *trans* in the crystal) and $\beta 4$ (*trans* in the gel versus *gauche* in the crystal).

It has usually been assumed for the purpose of interpreting experimental data that the hydrocarbon chains are all-*trans* and rotationally disordered in the gel phase, and hence can be regarded as cylinders, because the wide-angle x-ray peaks are confined to the (20) and (11) Bragg rods (Nagle, 1993). Using x-ray diffraction and infrared spectroscopic data, Nagle (1993) extracted the value -0.30 for the chain rotational order parameter, $g = \langle 2\cos^2\gamma - 1\rangle$, where γ is the angle between the zigzag plane of the chain carbon atoms and the plane defined by the tilt direction. Assuming a δ-function distribution, this corresponds to $\gamma = 54°$. Note that, with this assumption, $g = 1$ corresponds to $\gamma = 0°$ (parallel to tilt plane) and $g = -1$ to $\gamma = 90°$ (perpendicular to tilt plane). Thus, the small value of g obtained by Nagle is consistent with the usual picture of chain rotation disorder. However, Nagle also discussed the possibility that distinct orientational populations could exist, such that the resulting g happens to be small, in which case there would be relatively little rotational disorder in the hydrocarbon chains. To investigate this possibility, we calculated g from the MD run separately for each of the two DPPC hydrocarbon tails and obtained the values -0.36 for the *sn*-1 chain and -0.66 for the *sn*-2 chain. The average values of γ are 58° and 68°, respectively. Averaged over the two chains, $g = -0.47$ and $\gamma = 63°$. Assuming a δ-function distribution, the average value of g from the simulation gives $\gamma = 59°$, which agrees well with the value extracted by Nagle from experimental data. The values of γ for the individual methylene groups are fairly constant throughout the hydrocarbon chains, except at the ends, where γ tends toward slightly smaller values.

Upon closer inspection, we found that the *sn*-1 chain has two preferred orientations: the plane defined by the chain backbone carbon is either perpendicular or parallel to the

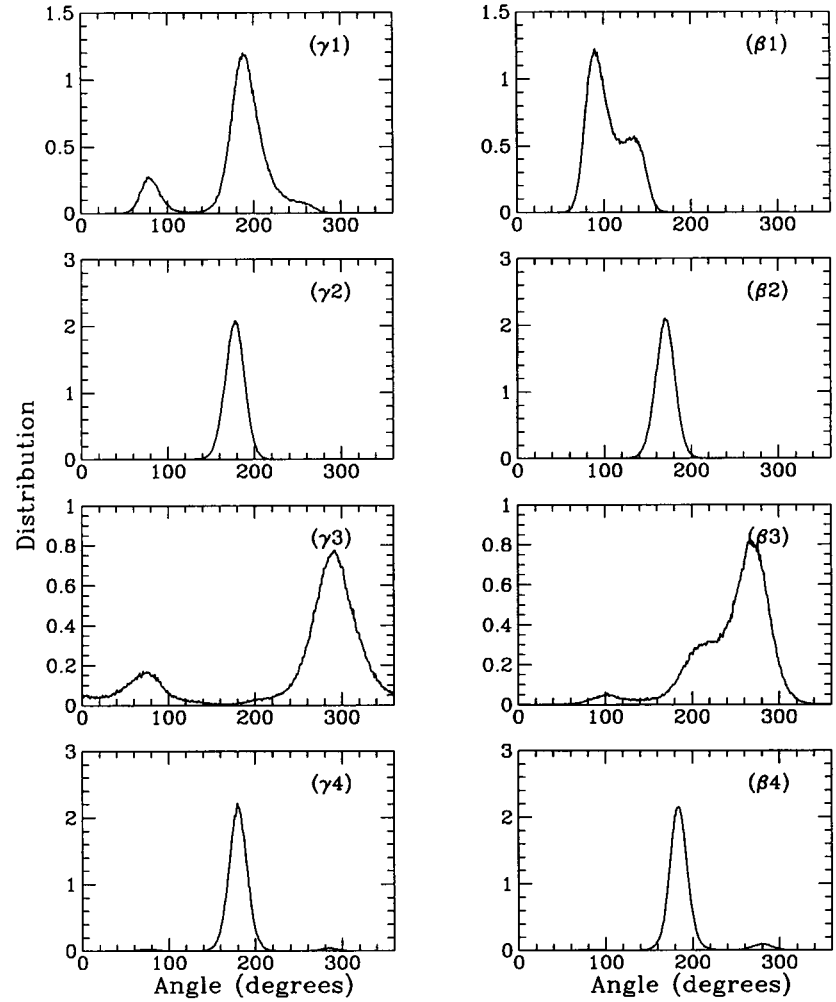

FIGURE 10 The torsional probability distributions for the acyl ester region. The notation is given in Fig. 11.

plane defined by the tilt direction and the bilayer normal, and the perpendicular/parallel ratio is 2.4. In contrast, the ratio for the *sn*-2 chain is 7, i.e., there is one predominant orientation perpendicular to the tilt plane. We calculated the correlation times for the rotational jump of the two types of chains and found that the interchange rate between the two rotational states for the *sn*-1 chain is faster than for the *sn*-2 chain. This is in spite of the fact that the *sn*-1 chain is more ordered at the C2 position, a conclusion that follows from the larger NMR order parameter of the *sn*-1 chain at C2 (Seelig and Seelig, 1974) and is verified by our simulation. We also found that, on the average, the zigzag planes of the two hydrocarbon chains in a given DPPC molecule are mostly parallel to one another: the parallel/perpendicular ratio is 3:1. The relative orientation of the chains may be related to the tilt direction.

To complete the characterization of the hydrocarbon chain structure, we have analyzed the chain conformations and found that there are 2, 3, 3, 4, 10, and 18% *gauche* defects in the last six bonds below the acyl ester linkages (C8-C9, . . . , C14-C15), respectively, and essentially 0% in the rest. This finding agrees with deductions from neutron and other experiments (Pfeiffer et al., 1989; Yellin and Levin, 1977), and means that the chains are nearly all-*trans* in the gel phase.

The detailed knowledge of the headgroup conformations and interactions with each other and with the solvent is prerequisite for understanding the functional properties of the headgroup/water interface. A lot of effort has been devoted to the interpretation of the preferred conformations in the gel and liquid crystal phases. Hauser et al. (1981) made some predictions according to the available single crystal structures and x-ray diffraction, neutron scattering, and NMR data on lipid bilayers. The MD simulation provides direct information on the headgroup conformational equilibrium and solvation in the fully hydrated gel phase bilayer. We devote the remainder of the paper to these topics.

First, we compare the headgroup structures observed in the simulation with those in the DMPC crystal (Pearson and Pascher, 1979). The data in Table 4 show that the headgroup orientations and intramolecular geometries are similar in the crystal and gel phases. In the gel phase, the distances between the negatively charged phosphate and positively charged ammonium groups are slightly longer than in the crystal and, as discussed above, the headgroup dipoles have

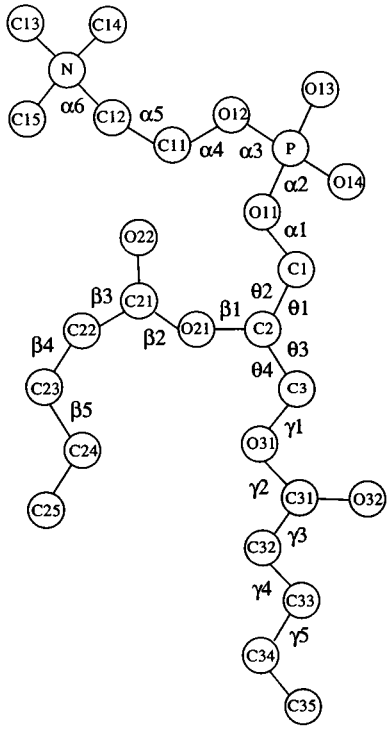

FIGURE 11 Notation for dihedral angles in lecithins (after Hauser et al., 1981).

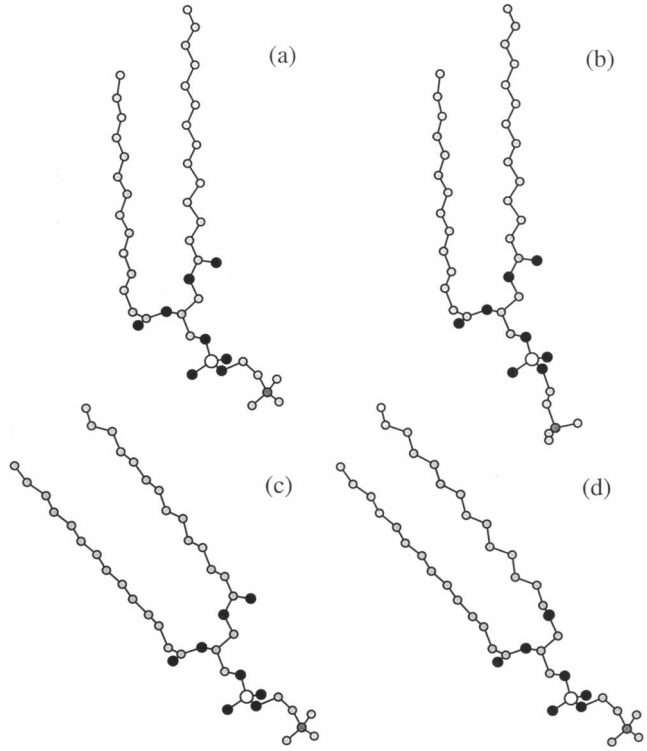

FIGURE 12 (*a*) DMPC molecule 1 from the crystal structure (Pearson and Pascher, 1979). (*b*) Generation of an upright headgroup by changing $\alpha 3$ and $\alpha 5$ to 180°. (*c*) Generation of tilted hydrocarbon chains by changing $\gamma 3$ to 300° and $\beta 4$ to 180° (as in the major MD population). (*d*) Generation of tilted hydrocarbon chains by changing $\gamma 1$ and $\gamma 3$ to 80° and $\beta 4$ to 180° (as in the minor MD population).

a broad orientational distribution (>20° rms fluctuation). These observations reflect the weakening of the intramolecular interaction between the phosphate and ammonium groups by hydration. Fig. 13 shows the dihedral angle distributions of the headgroup and glycerol region. For the most part, the preferred conformations in the DPPC gel phase are similar to those found in the two molecules in the DMPC crystal structure. The most notable differences from the crystal structure are in $\alpha 3$, $\alpha 5$, and $\alpha 6$. In the crystal, $\alpha 3$ and $\alpha 5$ are either *gauche*$^+$/*gauche*$^-$ or *gauche*$^-$/*gauche*$^+$. Both of these sets of conformations are populated (the latter only slightly) in the simulation; however, there is also a significant population (almost half) of *trans*/*trans*. Fig. 12 *b* shows that the effect of this *trans*/*trans* modification is to point the P-N vector away from the plane of the bilayer. The last significant difference is that $\alpha 6$, which is *trans* in the crystal, is almost exclusively *gauche*$^-$ in the gel.

Although the hydrocarbon chains exhibit a high degree of order in the gel phase, the headgroups appear to be disordered (see Fig. 7). To characterize the intermolecular interactions in disordered systems (such as liquids), it is useful to consider the radial distribution function, $g_{XY}(r)$, which is proportional to the probability of finding atom Y at a distance r from atom X. We have calculated the nitrogen-nitrogen and phosphorus-phosphorus radial distribution functions, $g_{NN}(r)$ and $g_{PP}(r)$, respectively, and plotted them in Fig. 14. Each $g(r)$ has two prominent peaks, at 6.6 and 8.8 Å for N-N, and 5.8 and 9.2 Å for P-P. Integration up to the first and second minima gives coordination numbers of 1.2 and 5.7 in the first two shells for nitrogen, and 2.3 and 6.9 for phosphorus. The phosphate groups are relatively more ordered, i.e., there is a larger first peak in $g_{PP}(r)$ compared

TABLE 4 Headgroup structure and orientation in the DPPC gel phase simulation and the DMPC crystal structure

	Inclination toward layer plane (°)			
	C (1)-C (2) bond	P-N dipole	PO_2^-–N dipole	P(O (13) O (14)) plane
DPPC	56 (10)	19 (24)	12 (24)	34 (22)
DMPC 1*	61	17	9	53
DMPC 2*	63	27	18	57
	Intramolecular distance (Å)			
	O (12)—N	P—N	O (13) O (14) N	PO_2^-—N
DPPC	3.5 (0.3)	4.7 (0.4)	5.3 (0.5) 5.0 (0.6)	5.0 (4)
DMPC 1*	3.2	4.3	5.2 4.1	4.5
DMPC 2*	3.2	4.5	5.3 4.3	4.7

The root-mean-squared fluctuations from the MD simulation are given in parentheses.

*From the DMPC crystal structure (Pearson and Pascher, 1979).

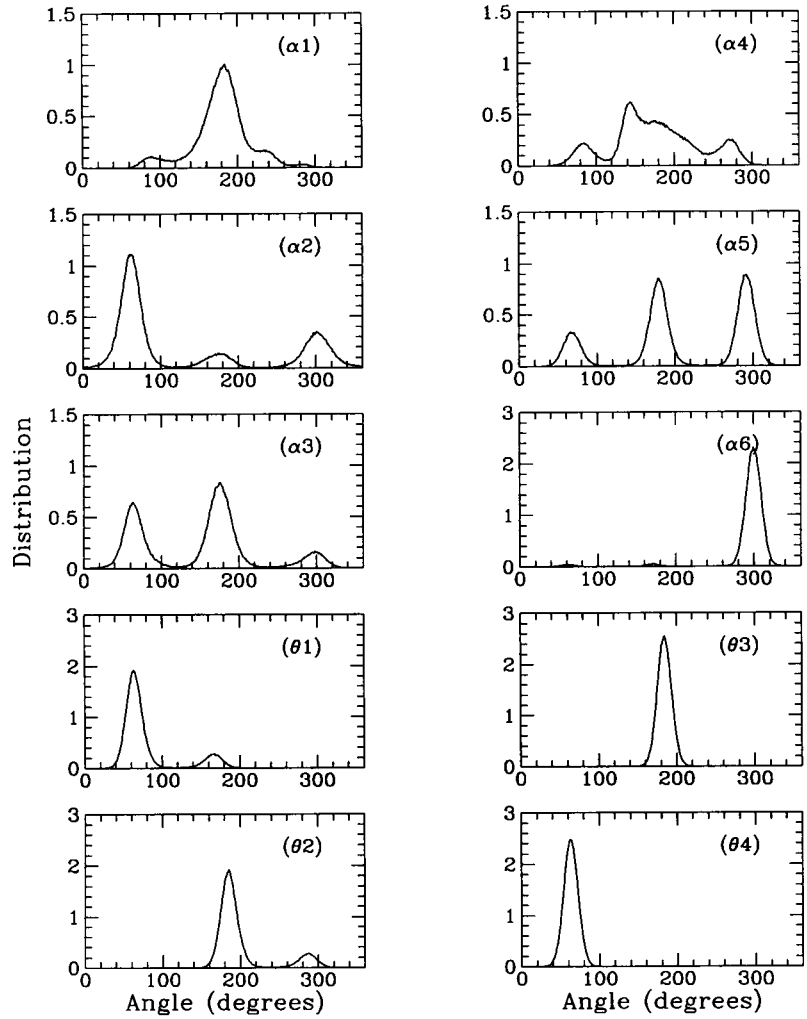

FIGURE 13 The torsional probability distributions for the headgroup and glycerol region. The notation is given in Fig. 11.

to $g_{NN}(r)$, because of the close packing of the hydrocarbon chains and the rigidity of the phosphate/glycerol connection. On the other hand, the flexibility of the choline group allows greater disorder in the ammonium groups, reflected in the smaller first peak in $g_{NN}(r)$, to avoid steric clashes and accommodate hydration of the polar moeities. The positions of the first peaks in $g_{NN}(r)$ and $g_{PP}(r)$ are systematically greater than the intermolecular distances in the DMPC crystal structure, which are 5.6 and 6.4 Å for N-N and 5.4 Å for P-P.

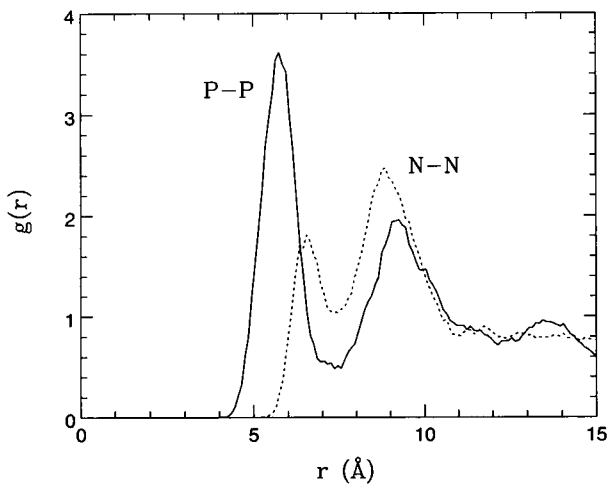

FIGURE 14 Phosphorus-phosphorus (*solid line*) and nitrogen-nitrogen (*dotted line*) radial distribution functions.

Now we turn to the interaction between the DPPC and water molecules. The electron density profiles in Fig. 4 show that the water molecules penetrate the glycerol ester region. We begin a more comprehensive analysis by considering the radial distribution functions plotted in Fig. 15 for the water oxygen atoms surrounding the phosphate phosphorus and oxygen, ammonium nitrogen, and carbonyl carbon atoms, respectively. There is a sharp first peak in the P-O_w $g(r)$ at 3.8 Å, indicating strong hydration of the phosphate group. Integration of this peak gives a coordination number of 3.7 water molecules for the first hydration shell. The N-O_w $g(r)$ displays a pronounced, but significantly broader first peak at 4.8 Å corresponding to 14.5 water molecules surrounding the ammonium group. We examined the probability distributions of the water coordination num-

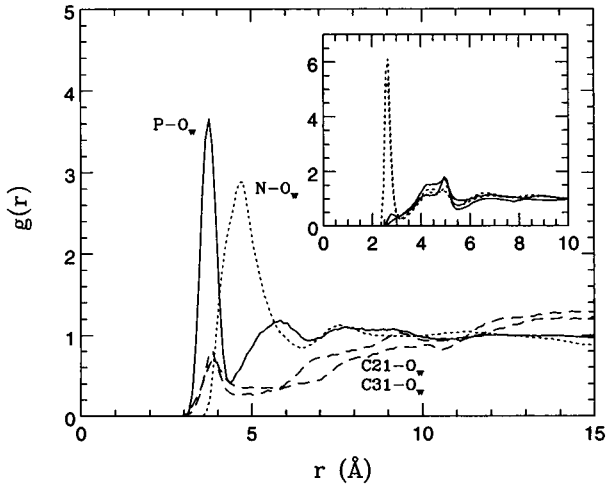

FIGURE 15 Radial distributions of water oxygen atoms around phosphorus (*solid line*), nitrogen (*dashed line*), and carbonyl oxygen (*dotted lines*) atoms. The inset shows the radial distributions of water oxygens around the ester (*solid lines*) and non-ester (*dotted lines*) phosphate oxygens.

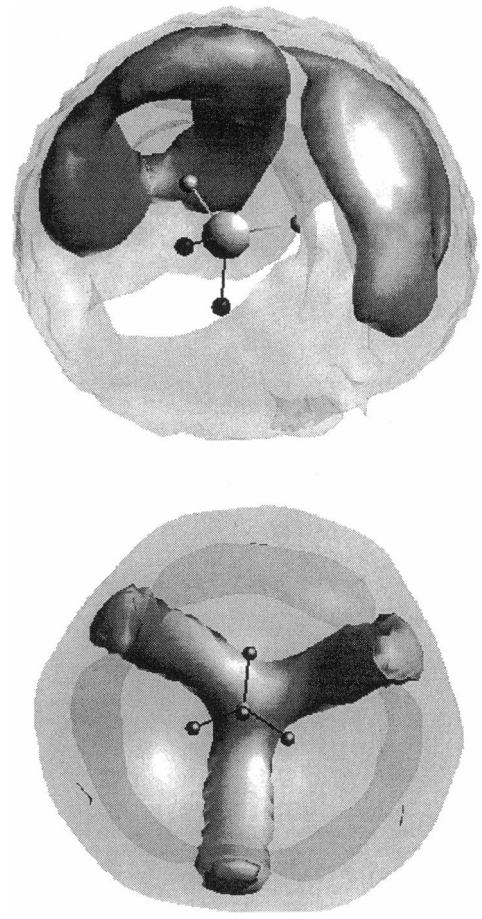

FIGURE 16 Density isosurfaces for water around the phosphate group, PO_4 (*upper*), and ammonium group, $CH_2N(CH_3)_3$ (*lower*). The darker contours correspond to the higher density.

ber (not shown) and found that the phosphorus distribution is sharply peaked at 3–4 waters whereas the nitrogen distribution is very broad, ranging from 4 to 30 waters. There is a drastic difference in the hydration of the esterified and nonesterified oxygen atoms in the phosphate group, as can be seen in the phosphate O-O_w $g(r)$ functions shown in the inset of Fig. 15: the water molecules are almost exclusively associated with the nonesterified oxygens. The position of the first peak of the O (nonester)-O_w, 2.6 Å, signals the presence of strong hydrogen bonds, and integration gives 1.6 hydrogen bonds per oxygen atom. The tiny first peaks in the carbonyl C-O_w $g(r)$ functions suggest that the carbonyl groups are very weakly hydrated. Integration of the first peaks (to 4.5 Å) gives 0.5 water in the vicinity of each ester group. This is in contrast to the situation in the liquid crystal phase, where the ester groups are well hydrated (Marrink and Berendsen, 1994; Tu et al., manuscript in preparation). Evidently, the close-packed arrangement of the hydrocarbon chains leaves relatively little room for water molecules in the carbonyl region of the gel phase.

To gain further insight into the three-dimensional arrangement of the water molecules around the headgroups, local density isosurfaces (Shelley et al., 1993) of the water oxygen atoms around the phosphate and ammonium groups were calculated and are plotted in Fig. 16. Only the first coordination shells (up to the first minima) in the radial distribution function are displayed, with the darker contours corresponding to the highest density. Fig. 16 *a* clearly shows the preferential hydration of the two nonesterified phosphate oxygen atoms. The higher-density contours form rings around the axes defined by the P-O (nonester) bonds, and evidently, this is the best way to distribute ~2 waters hydrogen bonded to each nonester oxygen. The density isosurface around the ammonium group shown in Fig. 16 *b* is generally more diffuse, although the higher-density contour shows that the water molecules closest to the nitrogen atom are highly concentrated in grooves between the methyl groups.

CONCLUSIONS

In conclusion, we have carried out a NPT MD simulation of a fully hydrated DPPC bilayer in the gel phase. Many aspects of the bilayer structure have been investigated. The results of the simulation were compared in detail with a variety of x-ray and neutron diffraction data. The average positions of specific carbon atoms along the bilayer normal were within the uncertainties of the values extracted from neutron data, and the interlamellar spacing and electron density profile were in very good agreement with low-angle x-ray diffraction results. The area per lipid and the details of the in-plane hydrocarbon chain structure (lattice parameters, chain tilt angle and direction, and chain offsets at the bilayer center) were in excellent agreement with the most detailed model used to date to quantitatively fit the latest wide-angle diffraction data. The only significant deviation is that the

chains met in a pleated arrangement at the bilayer center, although they should be parallel. It is likely that the pleated structure is a local free energy minimum in which the simulation was stuck as a result of the initial conditions. The overall quality of the results demonstrates that, after a relatively long equilibration period, a constant NPT simulation is capable of reproducing most known aspects of the gel-phase structure to atomic resolution and lends credibility to novel predictions in present and future simulations of lipid bilayers.

The novel discoveries made in the present work include the observation of a bimodal headgroup orientational distribution. Furthermore, we found that there is a significant number of *gauche* conformations near the ends of the hydrocarbon chains and, in addition to verifying a previous suggestion that there is partial rotational ordering in the hydrocarbon chains, that the two chains in a given molecule are inequivalent with respect to rotations: the *sn*-1 chains can be either parallel or perpendicular to the tilt plane, whereas the *sn*-2 chains are predominantly perpendicular. Finally, we have investigated the lipid/water interface and found that the water penetrates beneath the headgroups, but not as far as the carbonyl groups, that the phosphates are strongly hydrated almost exclusively at the nonesterified oxygen atoms, and that the hydration of the ammonium groups is more diffuse, with some water molecules concentrated in the grooves between the methyl groups. These and future predictions should be useful in the refinement of models used to interpret experimental data on lipid bilayers.

We are grateful to John Nagle, Wenjun Sun, Rich Pastor and Chris Mundy for helpful discussions, and to John Shelley and Mounir Tarek for assistance with the molecular graphics.

The research reported herein was supported by the National Institutes of Health through grants R01 GM40712 and F32 GM14463, and the National Science Foundation through grant DMR 91-20668. The calculations were performed on the Cray C90 at the Pittsburgh Supercomputing Center under Metacenter allocation MCA93S020.

REFERENCES

Allen, M. P., and D. J. Tildesley. 1989. Computer Simulation of Liquids. Oxford University Press, New York.

Berendsen, H. J. C., J. R. Grigera, and T. P. Straatsma. 1987. The missing term in effective pair potentials. *J. Phys. Chem.* 91:6269–6271.

Brooks, B. R., R. E. Bruccoleri, B. D. Olafson, D. J. States, S. Swaminathan, and M. Karplus. 1983. CHARMM: a program for macromolecular energy, minimization, and dynamics calculations. *J. Comp. Chem.* 4:187–217.

Büldt, G., H. U. Gally, J. Seelig, and G. Zaccai. 1979. Neutron diffraction studies on phosphatidylcholine model membranes. I. Headgroup conformation. *J. Mol. Biol.* 134:673–691.

Chiu, S.-W., M. Clark, V. Balaji, H. L. Scott, and E. Jakobssen. 1995. Incorporation of surface tension into molecular dynamics simulation of an interface: a fluid phase lipid bilayer membrane. *Biophys. J.* 69: 1230–1245.

Damodaran, K. V., K. M. Merz, and B. P. Gaber. 1992. Structure and dynamics of the dilauroylphosphatidylethanolamine lipid bilayer. *Biochemistry.* 31:7656–7664.

Egberts, E., S.-J. Marrink, and H. J. C. Berendsen. 1994. Molecular dynamics simulation of a phospholipid membrane. *Eur. Biophys. J.* 22:423–436.

Feller, S. E., Y. Zhang, and R. W. Pastor. 1995. Computer simulation of liquid/liquid interfaces. II. Surface tension-area dependence of a bilayer and a monolayer. *J. Chem. Phys.* In press.

Hauser, H., I. Pascher, R. H. Pearson, and S. Sundell. 1981. Preferred conformation and molecular packing of phosphatidylethanolamine and phosphatidylcholine. *Biochim. Biophys. Acta.* 650:21–51.

Heller, H., M. Schaefer, and K. Schulten. 1993. Molecular dynamics simulation of a bilayer of 200 lipids in the gel and in the liquid-crystal phases. *J. Phys. Chem.* 97:8343–8360.

Hentschel, M. P., and F. Rustichelli. 1991. Structure of the ripple phase $P_{\beta'}$ in hydrated phosphatidylcholine multimembranes. *Phys. Rev. Lett.* 66: 903–903.

Huang, P., J. J. Perez, and G. H. Loew. 1994. Molecular dynamics simulations of phospholipid bilayers. *J. Biomol. Struct. Dyn.* 11: 927–956.

Hui, S. W. 1976. The tilting of the hydrocarbon chains in a single bilayer of phospholipid. *Chem. Phys. Lipids.* 16:9–18.

Katsaras, J., D. S-C. Yang, and R. M. Epand. 1992. Fatty-acid chain tilt angles and directions in dipalmitoyl phosphatidylcholine bilayers. *Biophys. J.* 63:1170–1175.

Kenn, R. M., C. Böhm, A. M. Bibo, H. Möhwald, J. Als-Nielsen, and K. Kjaer. 1991. Mesophases and crystalline phases in fatty acid monolayers. *J. Phys. Chem.* 95:2092–2097.

König, S., E. Sackmann, D. Richter, R. Zorn, C. Carlile, and T. M. Bayerl. 1994. Molecular dynamics of water in oriented DPPC multilayers studied by quasielastic neutron scattering and deuterium-nuclear magnetic resonance relaxation. *J. Chem. Phys.* 100:3307–3316.

Lesslauer, W., J. E. Cain, and J. K. Blasie. 1972. X-ray diffraction studies of lecithin bimolecular leaflets with incorporated fluorescent probes. *Proc. Natl. Acad. Sci. USA.* 69:1499–1503.

Levine, Y. K. 1973. X-ray diffraction studies of membranes. *Prog. Surf. Sci.* 3:279–352.

Marrink, S.-J., and H. J. C. Berendsen. 1994. Simulation of water transport through a lipid membrane. *J. Phys. Chem.* 98:4155–4168.

Martyna, G. J., D. J. Tobias, and M. L. Klein. 1994. Constant pressure molecular dynamics algorithms. *J. Chem. Phys.* 101:4177–4189.

Nagle, J. F. 1993. Evidence for partial rotational order in gel phase DPPC. *Biophys. J.* 64:1110–1112.

Nosé, S., and M. L. Klein. 1983. Constant pressure molecular dynamics for molecular systems. *Mol. Phys.* 50:1055–1076.

Pearson, R. H., and I. Pascher. 1979. The molecular structure of lecithin dihydrate. *Nature.* 281:499–501.

Pfeiffer, W., Th. Henkel, E. Sackmann, W. Knoll, and D. Richter. 1989. Local dynamics of lipid bilayers studied by incoherent quasi-elastic neutron scattering. *Europhys. Lett.* 8:201–206.

Robinson, A. J., W. G. Richards, P. J. Thomas, and M. M. Hann. 1994. Headgroup and chain behavior in biological membranes: a molecular dynamics computer simulation. *Biophys. J.* 67:2345–2354.

Ruocco, M. J., and G. G. Shipley. 1982. Characterization of the subtransition of hydrated dipalmitoylphosphatidylcholine bilayers. X-ray diffraction study. *Biochim. Biophys. Acta.* 684:59–66.

Ryckaert, J.-P., G. Ciccotti, and H. J. C. Berendsen. 1977. Numerical integration of the cartesian equations of motion of a system with constraints: molecular dynamics of n-alkanes. *J. Comp. Phys.* 23: 327–341.

Safran, S. A. 1994. Statistical Thermodynamics of Surfaces, Interfaces, and Membranes. Addison-Wesley, Reading.

Seelig, A., and J. Seelig. 1974. Dynamic structure of fatty acyl chains in a phospholipid bilayer measured by DMR. *Biochemistry.* 13:4839–4845.

Shelley, J. C., M. Sprik, and M. L. Klein. 1993. Molecular dynamics simulation of an aqueous sodium octanoate micelle using polarizable surfactant molecules. *Langmuir.* 9:916–926.

Shinoda, W., T. Fukada, S. Okazaki, and I. Okada. 1995. Molecular dynamics simulation of the dipalmitoylphosphatidylcholine (DPPC) lipid bilayer in the fluid phase using the Nosé-Parrinello-Rahman NPT ensemble. *Chem. Phys. Lett.* 232:308–312.

Small, D. M. 1986. The Physical Chemistry of Lipids. Plenum Press, New York.

Smith, G. S., E. B. Sirota, C. R. Safinya, and N. A. Clark. 1988. Structure of the L_β phases in a fully hydrated phosphatidylcholine multimembrane. *Phys. Rev. Lett.* 60:813–816.

Stouch, T. R. 1993. Lipid membrane structure and dynamics studied by all-atom molecular dynamics simulations of hydrated phospholipid bilayers. *Mol. Simulation.* 10:335–362.

Stouch, T. R., K. B. Ward, A. Altieri, and A.-T. Hagler. Simulations of lipid crystals: characterization of potential energy functions and parameters for lecithin molecules. *J. Comp. Chem.* 12:1033–1046.

Sun, W.-J., R. M. Suter, M. A. Knewtson, C. R. Worthington, S. Tristram-Nagle, R. Zhang, and J. F. Nagle. 1994. Order and disorder in fully hydrated unoriented bilayers of gel phase dipalmitoylphosphatidylcholine. *Phys. Rev. E.* 49:4665–4676.

Tristram-Nagle, S., R. Zhang, R. M. Suter, C. R. Worthington, W.-J. Sun, and J. F. Nagle. 1993. Measurement of chain tilt angle in fully hydrated bilayers of gel phase lecithins. *Biophys. J.* 64:1097–1109.

Tu, K., D. J. Tobias, and M. L. Klein. 1995a. Constant pressure and temperature molecular dynamics simulations of crystals of the lecithin fragments: glycerylphosphorylcholine and dilauroylglycerol. *J. Phys. Chem.* 99:10035–10042.

Tu, K., D. J. Tobias, and M. L. Klein. 1995b. Constant pressure and temperature molecular dynamics simulation of a fully hydrated liquid crystal phase dipalmitoylphosphatidylcholine bilayer. *Biophys. J. 69*: 2558–2562.

Venable, R. M., Y. Zhang, B. J. Hardy, and R. W. Pastor. 1993. Molecular dynamics simulation of a lipid bilayer and of hexadecane: an investigation of membrane fluidity. *Science.* 262:223–226.

Wiener, M. C., R. M. Suter, and J. F. Nagle. 1989. Structure of the fully hydrated gel phase of dipalmitoylphosphatidylcholine. *Biophys. J.* 55: 315–325.

Yellin, N., and I. W. Levin. 1977. Hydrocarbon chain trans-gauche isomerization in phospholipid bilayer gel assemblies. *Biochemistry.* 16: 642–647.

Zaccai, G., J. K. Blasie, and B. P. Schoenborn. 1975. Neutron diffraction studies on the location of water in lecithin bilayer model membranes. *Proc. Natl. Acad. Sci. USA.* 72:376–380.

Zaccai, G., G. Büldt, A. Seelig, and J. Seelig. 1979. Neutron diffraction studies on phosphatidylcholine model membranes. II. Chain conformation and segmental disorder. *J. Mol. Biol.* 134:693–706.

Zhou, F., and K. Schulten. 1995. Molecular dynamics study of a membrane-water interface. *J. Phys. Chem.* 99:2194–2207.